Recovery of metal oxoanions from basic solutions using cooperative sorption – Separation of Na2MoO4 and NaOH

Laatikainen Markku, Laatikainen Katri, Heinonen Jari, Sainio Tuomo

DOI: 10.1016/j.cej.2018.02.070

Recovery of Metal Oxoanions from Basic Solutions Using Cooperative Sorption – Separation of Na_2MoO_4 and NaOH

Markku Laatikainen, Katri Laatikainen, Jari Heinonen, Tuomo Sainio

PII: S1385-8947(18)30281-X
DOI: https://doi.org/10.1016/j.cej.2018.02.070
Reference: CEJ 18549

To appear in: *Chemical Engineering Journal*

Received Date: 23 January 2018
Revised Date: 13 February 2018
Accepted Date: 14 February 2018

Please cite this article as: M. Laatikainen, K. Laatikainen, J. Heinonen, T. Sainio, Recovery of Metal Oxoanions from Basic Solutions Using Cooperative Sorption – Separation of Na_2MoO_4 and NaOH, *Chemical Engineering Journal* (2018), doi: https://doi.org/10.1016/j.cej.2018.02.070

Recovery of Metal Oxoanions from Basic Solutions Using Cooperative Sorption – Separation of Na_2MoO_4 and NaOH

Markku Laatikainen[a*], Katri Laatikainen[b], Jari Heinonen[a], Tuomo Sainio[a]

a) Lappeenranta University of Technology, School of Engineering Science, Laboratory of Separation Technology, Skinnarilankatu 34, 53850 Lappeenranta, Finland

b) Lappeenranta University of Technology, School of Engineering Science, Laboratory of Chemical Metrology, Skinnarilankatu 34, 53850 Lappeenranta, Finland

[*] Corresponding author. Phone: +358 504368886; e-mail: markku.laatikainen@lut.fi

Abstract

Chromatographic separation of molybdate oxoanions and NaOH was studied using cooperative sorption as a method to recover both Mo and the base as concentrated solutions. Commercial non-ionic microporous adsorbents composed of hyper-crosslinked polystyrene and cross-linked cellulose were investigated at 22 and 60 ^{o}C. For comparison, some separation tests were made also with ion exchange resins. Separation was modeled using rigorous thermodynamic treatment and an explicit sorption model. Good separation in batch column was obtained with the non-ionic cellulose adsorbent, while the polystyrene adsorbent and the ion exchangers give only moderate fractionation. Typical cooperative behavior was found in both cases but the sorption mechanisms are different. In the polystyrene adsorbent, uptake of the electrolytes separately and as binary mixtures can be explained in terms of electrostatic and steric exclusion of the constituent ions and no attractive interactions appear to be present. On the contrary, no steric exclusion operates in the cellulose adsorbent and separation is based on attractive interactions between NaOH and the weakly acidic hydroxyl groups of the polysaccharide chains. At the conditions used in this study, separation was not affected by molybdate polymerization taking place at low NaOH concentrations.

Keywords: Cooperative sorption; Molybdate oxoanions; NaOH; Microporous adsorbents

1. Introduction

Hydrometallurgical processing of primary and secondary resources frequently involves steps, where the target metal is dissolved as oxoanions in strongly basic solutions. Typical examples of such anions include $Al(OH)_4^-$, $B(OH)_4^-$, $Ge(OH)_3O^-$, ReO_4^-, MoO_4^{2-} and WO_4^{2-}. In some cases the product can be directly precipitated from the solution but often neutralization is required. Acid precipitation of ammonium molybdates from NH_4OH or NaOH solutions is a typical example. Such solutions are produced in dissolution of roasting residues, in desorption of molybdate from ion exchangers or adsorbents and in the stripping step after solvent extraction [1, 2]. Mo exists in basic solutions solely as tetrahedral MoO_4^{2-} anion but under neutral and acidic conditions, transition to octahedral geometry takes place. At the same time, tendency to form polymeric species like $Mo_7O_{24}^{6-}$ and $Mo_8O_{28}^{7-}$ increases [3]. Depending on the precipitation conditions, ammonium molybdates of different stoichiometry are finally obtained [2].

In this paper, we propose a simple method for efficient recovery of the base before precipitation with acid. This procedure allows recycling of the base to the dissolution step and leads to substantial decrease in acid consumption. The base is separated from the molybdate species using the co-operative sorption described in our earlier publication [4]. Steric exclusion of electrolytes in non-ionic microporous adsorbents was originally proposed by Davankov and co-workers [5-7]. Conventionally, steric exclusion is applied only on substances that have large difference in their molar masses. With microporous adsorbents, however, separation of even simple electrolytes like HCl and NaCl becomes feasible. Separation stems from the tendency of the common anion to distribute evenly between the bulk liquid and the pore-filling liquid. Equivalent amount of cation is required and the smaller H^+ is preferred in the pore liquid, while Na^+ concentrates in the bulk solution [5, 6]. This method was also applied to Na_2SO_4/NaOH separation that is similar to the case of this study and reasonably good separation was found using a microporous polystyrene resin [5].

In this paper, we show that qualitatively similar results are obtained in systems, where the cooperativity stems from attractive interactions rather than from exclusion. This finding opens up new possibilities for utilization of cooperativity as a separation method. It has been shown that cooperative sorption can be applied to very high solution concentration and/or adsorbent loadings [7] and no chemicals other than water are needed to run the process [8]. Moreover, dilution effects are small and in some cases, the components can be recovered at concentrations exceeding the feed values. These features are quite opposite to the practice of ion exchange that is conventionally used in electrolyte separations. Cooperative sorption is not feasible in treatment of dilute solutions and conventional adsorption or ion exchange are more amenable for removal of trace amounts of oxoanions [9, 10].

In this study, separation of Na_2MoO_4/NaOH mixtures is studied experimentally and by model calculations using two different microporous non-ionic adsorbents. We have previously used hyper-crosslinked polystyrene and densely crosslinked dextran gel in separation of strong and weak electrolyte pairs [4]. Good results were obtained with the polysaccharide resin and, therefore, a novel cellulose-based material (GH-25) was selected for this study because of its superior stability under basic conditions. The experimental data measured at 22 and 60 ^{o}C are correlated using the generalized Donnan model described previously [4]. For GH-25, dissociation of very weakly acidic hydroxyl groups in polysaccharide chains is included in the model to explain the high NaOH affinity. Dissociation of cellulose is well-known and it is used in synthesis of cellulose derivatives [11] but to the best of our knowledge, this property has not been utilized in separation technology. Some separation tests are also made using conventional cation exchangers as the adsorbent. Moreover, influence of molybdate polymerization on the separation efficiency is investigated, because formation of larger species is advantageous in separation based on molecular size.

2. Experimental

2.1 Materials

Macronet MN-270 is a microporous adsorbent composed of hyper-crosslinked polystyrene and it was obtained from Purolite Inc. Porous Cellufine GH-25 resin composed of densely crosslinked cellulose was supplied by JNC Corp. Both resins are considered as rigid materials containing permanent micropores and the properties are listed in Table 1. Some separation tests were also made using weak and strong cation exchange resins CA16G and CS24G obtained from Finex Oy. CA16G is an acrylic resin containing carboxylic groups and CS24G is sulfonated polystyrene resin. Both are densely crosslinked gel-type resins with no permanent porosity and they were used in Na form.

Table 1

Standard reagent grade chemicals (Na_2MoO_4, NaOH, NaCl, HCl) were used and the electrolyte solutions were prepared in purified water (> 0.1 µS/cm).

2.2 Methods

Water content was measured by drying the adsorbent samples after equilibrating with water and centrifugating for 15 min at 3000 min^{-1}.

The sorption isotherms were determined using frontal analysis (FA) and pulse-on-plateau (POP) methods [12]. The resin was packed in a glass column (ID 15 mm) and the bed volume (BV) was 35 mL. The column was attached to two HPLC pumps (Knauer) and the outlet stream was analyzed on-line for conductivity, refractive index (RI) and UV absorption. Bed temperature was controlled by water circulating in the column jacket. In FA measurements, the solute concentration was increased stepwise and the equilibrium uptake was calculated from the midpoint of the front. When the new equilibrium state was attained, a small pulse (0.1-0.2 mL) of an aqueous solution containing 1.5 g/L of blue dextran (GE Health Care, molar mass about 3 MDa) and 5 g/L of methanol was injected. The position of the negative RI peak gave the slope of the isotherm, i.e. dq_i/dc_i, where i stands for NaOH or Na_2MoO_4. The isotherm was then obtained by numerical integration. The bed porosity was calculated from the position of the BD peak. The bed porosity values $\varepsilon_b = 0.40$ and $\varepsilon_b = 0.41$ were obtained for the MN-270 and GH-25 beds, respectively, and the porosity was found to remain constant.

The methanol peak was used to estimate total porosity of the GH-25 bed and the value $\varepsilon_p = 0.61$ was obtained. Methanol was used instead of D_2O in order to avoid hydration interactions. For MN-270, this method failed because of substantial methanol adsorption on the adsorbent and the total porosity was measured using D_2O as probe. A value of $\varepsilon_p = 0.59$ was obtained and it seemed too high in view of the pore volume 0.2-0.4 mL/g given by the manufacturer. Therefore, distribution coefficients defined in Eq. (1) were measured for HCl, NaOH and NaCl and the results are shown in Fig. 1. Values below unity indicate presence of exclusion and if $k_D > 1$, the adsorbate has attractive interactions with the solid matrix.

$$k_{D,i} = \frac{q_i}{\varepsilon_p c_i} \qquad (1)$$

Figure 1.

The data suggest that HCl has practically unhindered access to the pore volume, while the sodium salts experience substantial exclusion even at high concentrations. The free passage of HCl has been observed also earlier [7] and the experimentally determined porosity ε_p = 0.59 seems thus correct. Same value was obtained at 22 and 60 ^oC.

Separation experiments were made using the above set-up including a fraction collector. Feed pulses of 40-75 mL (1.1-2.4 BV) were injected and eluted with water to obtain the outlet profiles. Samples were analyzed using Raman spectroscopy for molybdate species and pH measurements for NaOH. The standard glass electrode was calibrated using known concentrations of NaOH and Na_2MoO_4. Based on triplicate measurements of some points, the accuracy of the concentration determinations was estimated as ± 3 %.

Raman spectra were measured using Jobin Yvon-Horiba Labram microscope with 633 nm laser excitation. The sample was placed in a 20 µL glass capillary and the spectra were typically collected for 30 s. A known concentration of $NaNO_3$ was added and the intensities were corrected against the nitrate peak at 1050 cm^{-1}. Concentration of the monomeric MoO_4^{2-} was obtained from the Raman intensity of the peak at 896 cm^{-1} with an extinction coefficient of $2.94 \cdot 10^4$ L/mol. This was the only Mo species present at moderate and high NaOH concentrations but as proton concentration increases, the equilibrium shifts towards the octahedral polymeric species. According to Ozeki et al. [3], heptamer and protonated heptamer are formed according to Eq. (2) and they give new Raman peaks at 940 and 958 cm^{-1}, respectively. The speciation diagram at Mo concentration of 0.50 mol/L and at 25 ^oC is shown in Fig. 2.

$$\begin{aligned} 7MoO_4^{2-} + 8H^+ &\rightleftarrows Mo_7O_{24}^{6-} + 4H_2O, && \log\beta_7 = 53.6 \\ 7MoO_4^{2-} + 9H^+ &\rightleftarrows HMo_7O_{24}^{5-} + 4H_2O && \log\beta_{7,H} = 56.0 \end{aligned} \quad (2)$$

Figure 2.

Under the conditions of this study, no protonated heptamer or other species appearing at low pH values [3] were expected and the extinction coefficient was determined only for the heptamer. A series of 0.5 M Na_2MoO_4 solutions were prepared and pH adjusted to 6-9 using concentrated HCl. The Raman spectra were measured and analyzed by means of HypSpec program [13]. Using the known extinction coefficient of the monomer and the stability constants of Eq. (2), the spectrum of the heptamer was found by fitting. At 940 cm^{-1}, the heptamer extinction coefficient was $1.49 \cdot 10^5$ L/mol.

3. Theory

3.1. Equilibrium Model

Detailed description of the model is found elsewhere [4] and only the key points are discussed here. The phase equilibrium of a given component is written in terms of chemical potential including mixing, electrostatic, swelling and steric contributions. After eliminating the Donnan potential, the equilibrium condition of an electrolyte $A_{\nu_A}^{z_A} B_{\nu_B}^{z_B}$ can be written as follows.

$$\begin{aligned} (m_{p,AB}\gamma_{p,AB})^{\nu_{AB}} &= (m_{AB}\gamma_{AB})^{\nu_{AB}} K_{st,AB} \exp\left(-\frac{V_{m,AB}\pi}{RT}\right) \\ \nu_{AB} &= \nu_A + \nu_B \\ m_{AB} &= (m_A^{\nu_A} m_B^{\nu_B})^{1/\nu_{AB}} \\ \gamma_{AB} &= (\gamma_A^{\nu_A} \gamma_B^{\nu_B})^{1/\nu_{AB}} \\ K_{st,AB} &= (K_{st,A})^{\nu_A} (K_{st,B})^{\nu_B} \\ V_{m,AB} &= \nu_A V_{m,A} + \nu_B V_{m,B} \end{aligned} \quad (3)$$

Here, m is molality, γ is ionic activity coefficient, V_m is partial molar volume and ν is stoichiometric coefficient. R and T have their usual meanings. The subscript p refers to the pore solution. K_{st} is steric distribution coefficient discussed in detail below and π is swelling pressure.

The ionic activity coefficients were calculated using the Pitzer model as described earlier [4]. Besides the ion-ion interaction parameters, the model allows interactions between the ions and the adsorbent. These parameters were previously used to explain the notably non-linear uptake of NaOH in a cross-linked dextran [4]. In this study, a somewhat different approach is used to explain similar behavior observed in the cellulose-based GH-25. In both cases, the glucosidic hydroxyl groups, ROH, of the polysaccharide chains act as very weak acids with a p$K_{a,ROH}$ of 13.7 [14]. For strong bases like NaOH this provides an additional uptake mechanism and it can be formally written as follows.

$$R-OH + NaOH \rightleftarrows R-OH\cdots NaOH \qquad (4)$$

The apparent equilibrium constant of reaction (4) was obtained from $K_{a,ROH}$ and the water ionic product K_w as logK_{NaOH} = pK_w - p$K_{a,ROH}$. Using the equilibrium constant K_{NaOH}, a Langmuir-type correlation (Eq. (5)) is obtained and total uptake of NaOH is then $q_{NaOH} = \varepsilon_p c_{p,NaOH} + \rho_s Q_{ROH-NaOH}$, where c is the molar concentration. Conversion between molar and molal concentrations was made using a solution density estimated by the method of Li and Lee [15]. Details of the calculations have been reported earlier [4].

Neither $K_{a,ROH}$ nor the total amount of dissociable groups, Q^*_{ROH}, are known but in order to simplify calculations, a fixed value of 1.5 mol/kg was given to the latter and only $K_{a,ROH}$ was treated as an

adjustable parameter. Theoretical value for Q^*_{ROH} is 6.2 mol/kg assuming that one OH group of each glucoside unit dissociates [14].

$$Q_{ROH-NaOH} = \frac{Q^*_{ROH} K_{NaOH} a_{p,OH} a_{p,Na}}{1 + K_{NaOH} a_{p,OH} a_{p,Na}} \tag{5}$$

However, Eq. (5) proved to be insufficient to describe the cooperative effect of the common cation and it was replaced by an empirical correlation given in Eq. (6), where α is an adjustable parameter and K_{NaOH}^0 is the equilibrium constant at infinite dilution.

$$Q_{ROH-NaOH} = \frac{Q^*_{ROH} K_{NaOH} a_{p,OH}}{1 + K_{NaOH} a_{p,OH}} \qquad K_{NaOH} = K^0_{NaOH}(1 + \alpha c_{p,Na}) \tag{6}$$

The swelling pressure π in Eq. (3) is assumed to vanish in rigid materials and the pressure of the pore fluid was taken equal to that of the bulk solution. The steric distribution coefficient, K_{st}, for spherical ions in cylindrical pores is obtained from Eq. (7) [16] and K_{st} was assumed independent of solution concentration. Here L_{ion} and L_p represent the diameter of the hydrated ion and the average pore diameter, respectively. Note that $K_{st} \in [0,1]$ with $K_{st} = 1$ meaning no steric exclusion from the pores.

$$K_{st,i} = (1 - \frac{L_{ion,i}}{L_p})^2 \tag{7}$$

In multicomponent systems, Eq. (3) is written for all electrolytes but not all expressions are independent. The molal concentrations of both phases are constrained by the electroneutrality

conditions given in Eq. (8), where z is the ion charge and subscript R refers to the fixed charges of the solid. For simplicity, the charges are assumed to be evenly distributed in the pore volume.

$$\begin{aligned} \sum_{ions} z_i m_i &= 0 \\ z_R m_{p,R} + \sum_{ions} z_i m_{p,i} &= 0 \end{aligned} \qquad (8)$$

When the composition of the bulk solution is known, equilibrium concentrations in the solid phase can be obtained by solving Eqs (3) - (8). Volume changes are not taken into account and the properties of the water-swollen materials are used, because actual variation in bed volumes under the studied conditions was less than 2 %.

The rigorous treatment outlined above gives physically meaningful description for cooperative sorption but because of iterative solutions needed, it is less suitable for process simulations. Therefore, an explicit expression to calculate the electrolyte uptake was also tested. The SRS (Scheindorf-Rebhun-Scheintuch) model reported by Scheindorf et al. [17] is a generalized Freundlich isotherm and can be written as follows. K_F and n_F are the Freundlich parameters and b is an interaction parameter. The unit concentration is given by c^0.

$$c_{p,i} = K_{F,i} c_i \left(\sum_j b_{ij} \frac{c_j}{c^0} \right)^{n_{F,i}-1} \quad \text{(i,j = } Na_2MoO_4\text{, NaOH)} \qquad (9)$$

3.2. Column Model

Axial concentration profiles in the column were calculated using a discrete model described in detail elsewhere [10], where the continuous resin bed is approximated by mixing stages in series. In this approach the partial differential mass balance equation is replaced by the ordinary differential

equation given in Eq. (10). Here c is the molar concentration, q is total uptake, u is interstitial flow velocity, t is time, ε_b is bed porosity and ρ_s is resin density. Moreover, the overbar indicates volume-averaged value (see below). N is the number of mixing stages, H_b is the length of the bed and k is the index of the stage (*i.e.* axial position). At k = 1, the concentrations are equal to the feed concentrations. The effect of axial dispersion was accounted for by adjusting the number of stages as described earlier [4].

$$\frac{dc_{i,k}}{dt} + u\frac{N(c_{i,k} - c_{i,k-1})}{H_b} + (\frac{1-\varepsilon_b}{\varepsilon_b})\rho_S \frac{d\bar{q}_{i,k}}{dt} = \nu_i r_{pol}$$

$$r_{pol} = k_{pol}\left[\left(\frac{c_{Na_2MoO_4}}{c^0}\right)^7 - \frac{1}{K_{pol}}\left(\frac{c_{Na_6Mo_7O_{24}}}{c^0}\right)\left(\frac{c_{NaOH}}{c^0}\right)^8\right] \qquad (k = 2\ldots N) \qquad (10)$$

The reaction term was added to include the molybdate polymerization reaction (Eq. (1)) and ν is stoichiometric coefficient. For simplicity, only Na_2MoO_4 (ν = -7) and the heptamer (ν = 1) were taken into account and Eq. (2) was rewritten as follows to include the NaOH concentration.

$$7MoO_4^{2-} + 4H_2O \rightleftarrows Mo_7O_{24}^{6-} + 8NaOH, \qquad \log K = \log\beta_7 - 8\log K_w \qquad (11)$$

The rate constant k_{pol} = $1.0\cdot10^{-3}$ mol/Ls was adjusted to ensure reaction equilibrium at every calculation point. The following parameters were used for the heptamer: $K_{st,\ Mo7O24}$ = 0.8 and $D_{p,Mo7O24}$ = $1.0\cdot10^{-12}$ m^2/s.

The accumulation rate of the electrolytes in the solid phase was described using the linear driving force (LDF) approximation [4] and neglecting the external mass transport resistance. Consequently, the intra-particle concentration profiles are replaced by volume-average concentrations and Eq. (12) is obtained. R_p is the average radius of the spherical adsorbent particles and the asterisk refers to the

pore entrance. The adsorbed amount Q is equal to 0 except for NaOH in GH-25, where it is obtained from Eq. (5).

$$\frac{d\overline{q}_i}{dt} \approx \frac{15\varepsilon_p D_{p,i}}{R_p^2}(c_{p,i}^* - \overline{c}_{p,i}) \qquad (12)$$
$$\overline{q}_i = \varepsilon_p \overline{c}_{p,i} + \rho_s \overline{Q}_i$$

The asterisk refers to the pore entrance, where the external solution concentration and the pore concentration are related via the equilibrium condition given in Eq. (3).

3.3 Calculations

The differential equations shown in Eqs (10) and (12) were solved using the methods described earlier [10]. The set of algebraic equations was solved by means of the Newton method and the Simplex method was used in parameter estimation. The initial and boundary conditions for a column experiment involving both loading and elution steps are as follows.

$$t = 0: \quad c_i = c_i^{eluent}, \quad \overline{c}_{p,i}^* = \quad c_i^{eluent}$$

$$0 < t \le t_{feed}: c_i(k=1) \quad = \quad c_i^{feed}$$

$$t > t_{feed}: c_i(k=1) \quad = \quad c_i^{eluent}$$

The superscripts “eluent” and “feed” refer to the water eluent and the feed pulse of the electrolyte solution. Correlation between the number of mixing stages N and the axial dispersion coefficient

was calculated as described previously [4]. For example, the estimated dispersion coefficient for the runs with GH-25 was $2 \cdot 10^{-7}$ m^2/s and thus the breakthrough curves were calculated using $N = 350$.

Goodness-of-fit was evaluated by the average relative deviation (ARD) defined in Eq. (13), where N_{dp} is the number of data points.

$$ARD = \frac{1}{N_{dp}} \sum_{j=1}^{N_{dp}} \left| \frac{q_{j,\exp} - q_{j,calc}}{q_{j,\exp}} \right| \times 100\% \qquad (13)$$

The Pitzer parameters at 25 ^{o}C were taken from Kim and Frederick [18]. At 60 ^{o}C, parameters for NaOH have been reported by Reynolds et al. [19] and the values for Na_2MoO_4 were taken from Ref. [20]. The ion product of water was calculated from the correlation of Marshall and Franck [21].

4. Results and Discussion

Separation studies were made in batch-pulse mode with MN-270 and GH-25 and the results are discussed in Section 4.1. The results were correlated with the model outlined in Section 3 and the pertinent parameters were determined as much as possible from independent measurements. Therefore, results from equilibrium measurements and from single-component pulse experiments are discussed in detail in Sections 4.2 and 4.3 and the separation results are analyzed in the light of these data. Finally, the explicit SRS model is compared with the model of this study in Section 4.4.

4.1 Separation Experiments

Results from separation experiments made with the two non-ionic adsorbents at 22 or 60 ^{o}C are shown in Fig. 3. A very large pulse of a mixture containing 0.5 mol/L of both Na_2MoO_4 and NaOH was injected and subsequently eluted with water. The continuous lines are model calculations and determination of the model parameters is discussed in later Sections. In general, the proposed model based on the cooperative mechanism explains well all the features observed experimentally. In details, however, the two systems are quite different as will be shown in Section 4.2.

Figure 3.

In both cases the pulse was large enough to saturate the bed and the outlet concentrations attained the feed values. Before that point, a fraction rich in molybdate was obtained and at the end, a NaOH-rich fraction eluted with substantial focusing. Focusing of both components is typically observed in cooperative systems [4, 7] and it is of practical importance, because the separated components can be recovered without dilution. This is in contrast with the usual case in chromatographic separations. For both resins, focusing of NaOH was much stronger and the maximum outlet concentration from the GH-25 bed was nearly twice the feed concentration. Even higher concentration effect was observed when the feed contained 0.1 mol/L of NaOH and 0.9 mol/L of Na_2MoO_4 (Fig. 4). In this case the maximum NaOH concentration was nearly 5 times the feed value and even the average NaOH-fraction concentration well exceeded the feed concentration (see below).

Figure 4.

As shown in Fig. 3, the situation is qualitatively similar for both adsorbents but separation of the fronts was much better with GH-25. This is due to different separation mechanisms; in MN-270 the two electrolytes separate because of steric exclusion from the pore volume, while attractive

interactions between NaOH and the adsorbent are the basis for separation in GH-25. The common factor that explains the similar shape of the profiles in Fig. 3 is cooperation via the common cation Na^+. This means that uptake of the individual electrolytes is coupled through the generalized Donnan equilibrium (Eq. (3)) or the concentration-dependent binding constant of NaOH (Eq. (6)). A more detailed discussion of the mechanisms is given in the following Section.

It is evident from Fig 3A that simple batch separation with MN-270 is not feasible and more advanced process configurations like steady-state recycling chromatography [22] or simulated moving bed (SMB) [23] are needed. On the other hand, batch separation into nearly neutral molybdate fraction and Mo-free NaOH fraction is possible using GH-25 as shown in Figs 3B and 4. Furthermore, the electrolytes are recovered practically without dilution or even at concentrations above the feed concentration. Using the data of Fig. 4 and excluding the saturation section, the following simple process scheme can be constructed. A 1.80 BV pulse containing 0.9 mol/L of Na_2MoO_4 and 0.10 mol/L of NaOH is fed in the bed during the loading step and subsequently eluted with water during the elution step. The steps may follow in a single bed or (as shown in the scheme 1) two beds are used to obtain a continuous operation. Na-molybdate is recovered with a 96 % yield as a nearly neutral solution, where the concentration is close to the feed value. For NaOH, the yield is 97 % and the average outlet concentration is as high as 0.35 mol/L.

Scheme 1.

Influence of Polymeric Molybdates

In the experiments discussed above, formation of polymeric molybdates was not observed. The molybdate front eluted at pH 7-8 and according to Fig. 1, this is too high for the polymerization reaction (Eq. (2)) to proceed. In one experiment, the MN-270 bed was first treated with 0.5 M HCl

and washed with water, and then the run shown in Fig. 3A at 60 ^{o}C was repeated. The outlet profiles were identical, except for the initial part of the molybdate front, where small amount of the heptamer was observed (Fig. 5). Near the molybdate breakthrough, outlet pH was below 6 and thus the conditions favor polymerization. However, the heptamer concentration was small and had no practical effect on molybdate separation. Model calculations gave qualitatively correct predictions but the amount of the heptamer was smaller than found experimentally, probably because the acid present in the resin was not explicitly accounted for in calculations. Because of the marginal significance of the heptamer formation, no further attempts were made to adjust the parameters.

Figure 5.

Separation with Charged Adsorbents

Separation of acids and neutral salts with ion exchange resins has been known since the findings of Nelson and Kraus [24]. By analogy, it may be possible to separate a base from a neutral salt using cation exchangers in the form of the common cation. Therefore, separation runs at similar conditions as discussed above were made with weak and strong cation exchangers, both in Na form. The sulfonic acid resin CS24G gave practically no separation but the concentration profiles obtained with the carboxylic acid resin CA16G (Fig. 6) are qualitatively similar to those of the non-ionic adsorbents.

Figure 6.

There are, however, two important differences; the molybdate front is broader and strong tailing is found in the NaOH peak thus making separation less efficient. Both these factors decrease the separation efficiency. The front flattening is due to electrolyte exclusion by the ionized acid groups

and the tailing is tentatively explained by the presence of small amount of very weakly acidic groups in the resin. It is well-known that the acidity of groups attached to a polymer backbone depends on the degree of dissociation. Ionization of the last groups becomes difficult because of the electrostatic interactions between the neighboring groups. However, such groups can act as sorption sites for NaOH in the same way as the cellulosic hydroxyl groups in GH-25 but because of higher acidity, adsorption is stronger and more pronounced tailing is observed.

Preliminary model calculations were made to test this hypothesis and the results are shown in Fig. 6. The amount of adsorption sites was taken as 0.10 mol/kg that is roughly 1 % of all acid groups and other parameters estimated by trial-and-error are given in Table 3. As seen in Fig. 6, predictions of NaOH tailing as well as the shoulder in molybdate front at about 0.5 BV are qualitatively correct. The latter stems from the cooperative effect of NaOH on Na_2MoO_4 and it disturbs the concave front shape typical for electrolyte exclusion.

4.2 Equilibrium Uptake

As discussed in earlier papers [4, 22], co-operative separation mainly stems from equilibrium properties. Therefore, equilibrium uptake of NaOH and Na_2MoO_4 was studied in detail both separately and from binary mixtures of different composition. The distribution coefficients obtained for NaOH and Na_2MoO_4 at 22 and 60 ^oC are depicted in Figs 7 and 8. The data for mixed solutions were measured at a total concentration of 1.0 mol/L. All isotherms were measured under conditions, where Mo is exclusively in the form of sodium molybdate and no attempts were made to determine the model parameters for the polymeric species.

Model calculations are given as continuous lines for pure components and as crosses/plusses for mixtures. The parameters listed in Table 2 were estimated by simultaneous fitting in the data measured for pure and mixed electrolytes. The average relative deviation calculated from Eq. (13) was 8.8 % (N_{dp} = 21) and 4.2 % (N_{dp} = 19) for MN-270 at 22 and 60 ^{o}C, respectively. The corresponding values for the GH-25 resin were 7.7 % (N_{dp} = 27) and 3.8 % (N_{dp} = 24).

Figure 7.

Figure 8.

Table 2.

The single-component isotherms shown in Figs 7A and 8A for MN-270 are qualitatively similar to those observed earlier [4] and they suggest that steric exclusion is the main cause for separation observed in Fig. 3A. Marked exclusion effect (k_D < 1) was found for both electrolytes and, quite interestingly, exclusion appears to decrease with increasing temperature. In principle, steric exclusion is an entropic process and should be insensitive to temperature changes. Weaker exclusion at 60 ^{o}C may therefore indicate changes in pore dimensions and/or degree of ion hydration. The low distribution coefficients at low concentrations can be explained by electrostatic repulsion between the electrolytes and the ionic groups present in the adsorbent. The calculated curves were obtained using a fixed charge density $m_{p,R}$ = 0.03 mol/kg.

Adsorption properties of the cellulose-based GH-25 are quite different. No steric exclusion seems to be present and the distribution coefficient of Na_2MoO_4 is close to unity, except for the low concentrations, where weak electrostatic repulsion by the fixed charges ($m_{p,R}$ = 0.015 mol/kg) decrease the k_D values. On the other hand, GH-25 has very high affinity for NaOH and as discussed

in Section 3.1., NaOH is assumed to be bound on the weakly acidic hydroxyl groups of the cellulose chains. Because of very low acid strength of the groups, binding is easily reversible and it is considered here as electrolyte adsorption rather than ion exchange (see Eq. (4)).

As discussed in detail in our earlier paper [4], the relative simple sorption pattern of the pure components becomes more complicated in mixtures because of cooperation (see Figs 7 and 8). The cooperativity means here that there is an exclusion/attraction affecting differently the two anions, OH^- and MoO_4^{2-} and the uptake of the two electrolytes is coupled via the common cation, Na^+. In the MN-270 case, the molybdate anion and the common counter-ion Na^+ are partly excluded, while OH^- is much less influenced. As a result, the distribution coefficient of Na_2MoO_4 decreases in the presence of NaOH and the reverse is true for NaOH in mixtures with Na_2MoO_4. Qualitatively similar cooperative effect was also found for GH-25, where no steric exclusion is present. As shown in Fig. 6, uptake of NaOH is strongly enhanced in the presence of Na_2MoO_4 and this is explained here by the influence of the common cation on the dissociation of the cellulosic hydroxyl groups (Eq. (5)). The increased sorption of NaOH is accompanied by enhanced exclusion of Na-molybdate in the presence of NaOH (Fig. 8B) exactly as in the case of steric exclusion. It should be noted that distribution of the electrolytes depend also on the mixing effects [24] and they are described by the activity coefficients calculated by the Pitzer model. Same parameters were used for the bulk and pore solutions.

The main separation mechanism in MN-270 was identified as steric exclusion and in fact, the experimental data could be explained using only the K_{st} parameters that depend on the relative dimensions of the ion and pore, L_{ion}/L_p (Eq. (7)). At 25 ^oC, for example, parameter estimation gave L_{Na}/L_p = 0.48 and L_{MoO4}/L_p = 0.44, while the corresponding hydrated ion diameters are 0.44 and 0.60 nm as estimated from the data of Marcus [26, 27]. It is well-known, however, that there is no unambiguous measure for the hydrated ion size or hydration numbers and according to Nightingale

[28], the hydrated diameters are much closer, i.e. 0.72 nm for Na^+ and 0.77 nm for MoO_4^{2-}. When the data measured at 60 ^oC were used, the estimated values were $L_{Na}/L_p = 0.25$ and $L_{MoO4}/L_p = 0.50$. It is probable that no simple correlation between the estimated parameters and hydrated ion size exists but they include also contribution from unknown factors present in the nano-scale fluid-solid system.

For GH-25, selective uptake of NaOH is based on attractive interactions with the adsorbent and $pK_{a,ROH}^0$ and α are the key parameters. Quite surprisingly, the equilibrium data could be explained reasonably well using only these two values, while L_{ion}/L_p was set to 0 for all ions and all ion-adsorbent interactions were neglected. Moreover, the value obtained for $pK_{a,ROH}^0 = 13.8$ at 22 ^oC is close to the value 13.7 determined experimentally [14].

In summary, analysis of the equilibrium data clearly show that the two systems are mechanistically different although the cooperative effect observed is qualitatively similar in both cases. Sorption in MN-270 can be described satisfactorily using only the steric exclusion parameters of the constituent ions. On the other hand, no steric exclusion is present in GH-25 and two parameters related to the adsorbent rather than the electrolytes are sufficient to correlate the uptake data. No indication of attractive interactions between the molybdate anion and the adsorbents was found, and the uptake is controlled by sterically hindered or unhindered partitioning between the bulk solution and the pore solution.

4.3 Estimation of Diffusion Coefficients

At conditions used in this study, mass transfer effects play only a minor role and the intra-particle diffusion coefficients were estimated by trial-and-error from the separation data and they are given in Table 3. External mass transfer resistance was neglected because of the high electrolyte

concentrations. The estimated D_p values were further tested against single-component frontal profiles measured at flow rates of 2-12 BV/h. The experimental and calculated data obtained for NaOH in MN-270 at 60 ^oC are shown in Fig. 9.

Table 3.

Figure 9.

The experimental results indicate that NaOH uptake in MN-270 is practically independent on the feed rate up to 6 BV/h, while significant front broadening takes place at 12 BV/h. The influence of the flow rate was less obvious for GH-25 (not shown) and it can be explained by the much smaller average particle size. The profiles obtained with Na_2MnO_4 were qualitatively similar but the estimated pore diffusion coefficients were about 5 times lower. Satisfactory correlation of the data was obtained with the approximate LDF model (Eq. (12)) because the uptake of NaOH and Na-molybdate deviates only moderately from a linear isotherm.

4.4 Data Correlation Using the SRS Model

Finally, the SRS model (Eq. (8)) was used for correlation of the equilibrium data and simulation of the breakthrough profiles. For MN-270, the parameters given in Table 4 gave good correlation with the equilibrium data (AAD (22 ^oC) = 4.5 %, AAD (60 ^oC) = 7.2 %). The results were less satisfactory with GH-25 (AAD (22 ^oC) = 15.6%, AAD (60 ^oC) = 9.8 %) and the cooperative effect on NaOH was systematically underestimated. As an example, the estimated equilibrium parameters together with the diffusion coefficients of Table 3 were used to calculate the breakthrough profiles shown in Fig. 5 and the results are shown in Fig. 10.

Table 4.

Figure 10.

The SRS model gives practically as good correlation as the more rigorous treatment used in this study even though its parameters bear no physical significance. The main advantage of the SRS or any other explicit model is that the calculation load is much smaller; calculation of the profiles in Fig. 10 took 35 s with the SRS model and nearly 80 min with the rigorous model, when a standard laptop computer was used.

5. Conclusions

In this paper, we have shown that chromatographic separation based on cooperative sorption can be used to recover metal oxoanions from basic solutions. Separation of Na_2MoO_4 and NaOH was used as the model case and two microporous non-ionic adsorbents were used. MN-270 composed of hypercrosslinked polystyrene has moderate selectivity for NaOH and separation stems from differences in steric exclusion of the constituent ions from the pore solution. Because of partial exclusion of both electrolytes, the separation efficiency is quite low and fractionation in a batch column is not feasible. No evidence was found of the polymeric Mo species, except in runs where the adsorbent was pre-treated with acid. Cellulose-based GH-25 adsorbent, on the other hand, gives good separation and the two electrolytes can be recovered with high yield at concentrations comparable with the feed concentrations. Although no steric exclusion was present, qualitatively similar cooperativity was observed both in equilibrium data and in the dynamic breakthrough curves. In this case, the origin for the cooperativity lies in the common ion effect on dissociation of the cellulosic hydroxyl groups and thus on adsorption of NaOH. The proposed model gives physically reasonable description of the data but the iterative calculations makes it difficult to use in

process simulations. Therefore, an explicit sorption model was also tested and found suitable for such purposes.

Acknowledgements

Financial support from TEKES, Finland (CMEco and IX Hydro projects), Academy of Finland, the Research Foundation of the Lappeenranta University of Technology, the Magnus Ehrnrooth Foundation and the Finnish Cultural Foundation are gratefully acknowledged. The authors thank Mr. Toni Laurikainen for assistance in experimental work.

List of Symbols

a	activity, -
b	interaction parameter in Eq. (9), -
c	molar concentration, mol/L
d_p	average particle diameter, m
D_p	pore diffusion coefficient, m^2/s
k_d	distribution coefficient, -
k_{pol}	rate constant for the MoO_4^{2-} polymerization reaction, mol/Ls
K_a	dissociation constant, -
K_F	Freundlich parameter, -
K_{pol}	equilibrium constant for the MoO_4^{2-} polymerization reaction, mol/L
K_{st}	steric distribution coefficient, -
K_w	ion product of water, -
H_b	bed heigth, m
L_{ion}	hydrated ion diameter, nm

L_p	average pore diameter, nm
m	molal concentration, mol/kg
n_F	Freundlich exponent, -
N	number of mixing stages, -
q	total uptake, mol/L
Q	adsorbed amount, mol/kg
R	gas constant, 8.314 J/(molK)
t	time, s
T	temperature, K
u	interstitial velocity, m/s
V_m	partial molar volume, L/mol
x	axial coordinate, m
z	ion charge, -
α	adjustable parameter in Eq. (6), L/mol
ε_b	bed void fraction, -
ε_p	pore void fraction, -
γ	activity coefficient, -
ν	stoichiometric coefficient, -
π	swelling pressure, Pa
ρ_S	polymer content in swollen resin, kg/L

Subscripts and Superscripts

0	initial, pure component or infinite dilution value
feed	feed value

i, j, k	component
p	pore, pore solution
R	fixed charges
w	water

Abbreviations

ARD	average relative deviation
BV	bed volume
CA16G	weak acid cation exchanger
CS24G	strong acid cation exchanger
GH-25	Cellufine GH-25 adsorbent
HCPS	hypercrosslinked polystyrene
MN-270	Hypersol Macronet MN-270 adsorbent

References

1. Z. Zhao, J. Li, C. Cao, G. Huo, G. Zhang, H. Li, Recovery and purification of molybdenum from Ni–Mo ore by direct air oxidation in alkaline solution, Hydrometallurgy 103 (2010) 68–73.
2. T.A. Lasheen, M.E. El-Ahmady, H.B. Hassib, A.S. Helal, Molybdenum metallurgy review: Hydrometallurgical routes to recovery of molybdenum from ores and mineral raw materials, Miner. Process. Extract. Metall. Rev. 36 (2015) 145–173.
3. T. Ozeki, H. Kihara, S. Hikime, Studies of raman spectra and equilibria of isopolymolybdate ions in aqueous acidic solutions by factor analysis, Anal. Chem. 59 (1987) 945-950

4. M. Laatikainen, T. Sainio, Cooperative sorption of weak and strong electrolytes in microporous adsorbents, Microporous Mesoporous Mater. 239 (2017) 86-95.
5. V.A. Davankov, M.P. Tsyurupa, N.N. Alexienko, Preparative frontal size-exclusion chromatography of mineral ions on neutral hypercrosslinked polystyrene, J. Chromatogr. A 1087 (2005) 3-12.
6. V. Davankov, M. Tsyurupa, Chromatographic resolution of a salt into its parent acid and base constituents, J. Chromatogr. A 1136 (2006) 118-122.
7. V. Davankov, M. Tsyurupa, Z. Blinnikova, L. Pavlova, Self-concentration effects in preparative SEC of mineral electrolytes using nanoporous neutral polymeric sorbents, J. Sep. Sci. 32 (2009) 64-73.
8. S. Hellstén, J. Heinonen, T. Sainio, Size-exclusion chromatographic separation of hydroxy acids and sodium hydroxide in spent pulping liquor, Separ. Purif. Technol. 118 (2013) 234-241.
9. S. Yu, X. Wang, H. Pang, R. Zhang, W. Song, D. Fu, T. Hayat, X. Wang, Boron nitride-based materials for the removal of pollutants from aqueous solutions: A review, Chem. Eng. J. 333 (2018) 343-360.
10. M. Laatikainen, M. Sillanpää, T. Sainio, Comparison of process configurations for arsenic removal with ion exchange, Desalination Water Treat. 57 (2016), 13770-13781.
11. Anon., Cellulose and Its Derivatives, http://polymerdatabase.com/polymer%20classes/Cellulose%20type.html (accessed 15 December 2017).
12. G. Guiochon, S.D. Shirazi, A.M. Katti, Fundamentals of preparative and nonlinear chromatography, Academic Press, Boston, 1994, pp. 81-85.
13. P. Gans, A. Sabatini, A. Vacca, Investigation of equilibria in solution. Determination of equilibrium constants with the HYPERQUAD suite of programs, Talanta 431 (1996) 1739-1753.

14. H. Motomura, S.-H. Bae, Z. Morita, Dissociation of hydroxyl groups of cellulose at low ionic strengths, Dyes Pigments, 39 (1998) 243-258.

15. C. Li, H. Lee, Density calculation of electrolyte solutions with the solution osmotic pressure, Chem. Eng. Sci. 55 (2000) 655-665.

16. J.C. Giddings, E. Kucera, C.P. Russell, M.N. Myers, Statistical theory for the equilibrium distribution of rigid molecules in inert porous networks. Exclusion chromatography, J. Phys. Chem. 72 (1968) 4387.

17. C. Sheindorf, M. Rebhun, M. Sheintuch, A Freundlich-type multicomponent isotherm. J. Colloid Interface Sci. 79 (1981) 136–142.

18. H.-T. Kim, W.J. Frederick, Evaluation of Pitzer ion interaction parameters of aqueous electrolytes at 25 C. 1. Single Salt Parameters, J. Chem. Eng. Data 33 (1988) 177-184.

19. J. G. Reynolds, R. Carter, A. R. Felmy, A Pitzer Interaction Model for the $NaNO_3$−$NaNO_2$−NaOH−H_2O System from 0 to 100 °C, Ind. Eng. Chem. Res. 54 (2015) 3062−3070.

20. P. Ning, W. Xu, H. Cao, X. Lin, H. Xu, Determination and modeling for the solubility of Na_2MoO_4+2H_2O in the (Na^+ + MoO_4^{2-} + SO_4^{2-}) system, J. Chem. Thermodynamics 94 (2016) 67–73.

21. W. L. Marshall, E. U. Franck, Ion product of water substance, 0-1000 ^oC, 1-10.000 bars. new international formulation and its background, J. Phys. Chem. Ref. Data, 10 (1981) 295.

22. J. Heinonen, H. Niskakoski, T. Sainio, Chromatographic separation of ethyl-β-D-glucopyranoside and D-glucose with steady-state recycling chromatography, Separ. Purif. Technology 169 (2016) 262-272.

23. M. Laatikainen, T. Sainio, V. Davankov, M. Tsyurupa, Z. Blinnikova, E. Paatero, Modeling of size-exclusion chromatography of electrolytes on non-ionic nanoporous adsorbents, J. Chromatogr. A 1149 (2007) 245–253.

24. F. Nelson, K.A. Kraus, Anion-exchange studies. XXIII. Activity coefficients of some electrolytes in the resin phase, J. Am. Chem. Soc. 80 (1958) 4154-4161.

25. M. Laatikainen, T. Sainio, V. Davankov, M. Tsyurupa, Z. Blinnikova, E. Paatero, Chromatographic separation of a concentrated HCl–$CaCl_2$ solution on non-ionic hypercrosslinked polystyrene, React. Funct. Polymers 67 (2007) 1589–1598.

26. Y. Marcus, Ionic radii in aqueous solutions, Chem. Rev. 88 (1988) 1475-1498.

27. Y. Marcus, Thermodynamics of solvation of ions. Part 5. Gibbs free energy of hydration at 298.15 K, J. Chem. Soc. Faraday Trans. 87 (1991) 2995-2999.

28. E. R. Nightingale, Phenomenological theory of ion solvation. Effective radii of hydrated ions, J. Phys. Chem. 63 (1959) 1381- 1387.

List of Tables

Table 1. Properties of the water-swollen adsorbents. n.a. = not available

	MN-270	GH-25
Average particle size d_p, mm	0.7	0.1
Pore size L_p, nm	2-3	n.a.
Particle porosity ε_p, -	0.59[a]	0.61[a]
Density ρ_S, kg/L[b]	0.47	0.52
Water content, kg/kg	0.46	0.56

a) Calculated from the D_2O or methanol retention data.

b) Polymer content in the swollen resin. Estimated from the water sorption data.

Table 2. Equilibrium parameters appearing in Eqs (3) – (7) for the studied systems at 22 and 60 °C.

Adsorbent	$pK_{a,ROH}^0$		α		Electrolyte	L_{cation}/L_p		L_{anion}/L_p	
	22 °C	60 °C	22 °C	60 °C		22 °C	60 °C	22 °C	60 °C
MN-270	-	-	-	-	NaOH	0.4524	0.2459	0.2178	0.1479
					Na_2MoO_4	0.4524	0.2459	0.4955	0.5049
GH-25	13.81	12.80	2.700	2.205	NaOH	0[a]	0[a]	0[a]	0[a]
					Na_2MoO_4	0[a]	0[a]	0[a]	0[a]
CA16G-Na	-	9.00[a]	-	1.00[a]	NaOH	-	0.35[a]	-	0[a]
					Na_2MoO_4	-	0.35[a]	-	0.30[a]

a) Fixed value.

Table 3. Pore diffusion coefficients, D_p, of NaOH and Na_2MoO_4 in MN-270 and GH-25.

Adsorbent	Solute	D_p (22 °C), 10^{-10} m^2/s	D_p (60 °C), 10^{-10} m^2/s
MN-270	NaOH	6.0	10.0
MN-270	Na_2MoO_4	1.0	3.0
GH-25	NaOH	4.0	7.0
GH-25	Na_2MoO_4	0.8	2.0

Table 4. Equilibrium parameters for the SRS model at 22 and 60 ^{o}C.

Adsorbent	Electrolyte	logK_F		n_F		b_{ij}	
		22 ^{o}C	60 ^{o}C	22 ^{o}C	60 ^{o}C	22 ^{o}C	60 ^{o}C
MN-270	NaOH	-0.3840	-0.2174	1.167	1.109	12.70	68.19
	Na_2MoO_4	-0.6868	-0.4737	1.014	1.285	-0.9961	-0.7697
GH-25	NaOH	0.4334	0.3636	0.8012	0.8596	-0.1014	-0.1098
	Na_2MoO_4	0.05526	0.06643	1.081	1.0581	-0.1467	-0.3010

Figure Captions

Figure 1. Distribution coefficients of HCl (squares), NaOH (circles) and NaCl (triangles) in MN-270 at 60 ^{o}C. The k_D values are calculated with $\varepsilon_p = 0.59$.

Figure 2. Speciation of Na_2MoO_4 in a 0.5 M solution at 25 ^{o}C. MoO_4^{2-}: solid line; $Mo_7O_{24}^{6-}$: dashed line; $HMo_7O_{24}^{5-}$: dotted line.

Figure 3. Separation of an equimolar mixture of Na_2MoO_4 (circles) and NaOH (triangles) with MN-270 (A) and GH-25 (B). T = 22 ^{o}C (open symbols, solid lines), T = 60 ^{o}C (filled symbols, dashed lines). $c_{Na2MoO4}^{0} = c_{NaOH}^{0} = 0.50$ mol/L. A: feed flow rate 5.0 BV/h, pulse volume 1.1 BV; B: feed flow rate 6.0 BV/h, pulse volume 1.6 BV. Continuous lines are model calculations.

Figure 4. Separation of Na_2MoO_4 (circles) and NaOH (triangles) with GH-25. T = 60 ^{o}C, $c_{Na2MoO4}^{0}$ = 0.90 mol/L, c_{NaOH}^{0} = 0.10 mol/L. Feed flow rate 6.0 BV/h, pulse volume 2.4 BV. Continuous lines are model calculations.

Figure 5. Elution profiles for Na_2MoO_4 (circles) and $Na_6Mo_7O_{24}$ (triangles) in acid-treated MN-270 bed. T = 60 ^{o}C; $c_{Na2MoO4}^{0} = c_{NaOH}^{0} = 0.50$ mol/L; feed flow rate 6.0 BV/h, pulse volume 1.6 BV. Continuous lines are model calculations.

Figure 6. Elution profiles for Na_2MoO_4 (circles) and NaOH (triangles) in CA16G-Na bed. T = 60 ^{o}C; $c_{Na2MoO4}^{0}$ = 1.0 mol/L, c_{NaOH}^{0} = 0.50 mol/L; feed flow rate 2.4 BV/h, pulse volume 0.40 BV. Continuous lines are model calculations.

Figure 7. Equilibrium uptake of NaOH at 22 (circles, solid lines, crosses) and 60 ^{o}C (triangles, dotted lines, plusses) from pure NaOH solutions and mixed Na_2MoO_4/NaOH solutions. A: MN-270; B: GH-25. Open symbols and continuous lines refer to experimental and calculated values for pure solutions. Filled symbols are the experimental values for mixtures with c_{tot} = 1.0 mol/L and crosses/plusses refer to the corresponding model calculations.

Figure 8. Equilibrium uptake of Na_2MoO_4 at 22 ((circles, solid lines, crosses) and 60 ^{o}C (triangles, dotted lines, plusses) from pure NaOH solutions and mixed Na_2MoO_4/NaOH solutions. A: MN-270; B: GH-25. Open symbols and continuous lines refer to experimental and calculated values for pure solutions. Filled symbols are the experimental values for mixtures with c_{tot} = 1.0 mol/L and crosses/plusses refer to the corresponding model calculations.

Figure 9. Estimation of the intra-particle diffusion coefficients from the frontal data of NaOH at 60 ^{o}C. Adsorbent MN-270, flow rate 1.8 BV/h (open triangles, dotted line), 5.1 BV/h (filled triangles, dashed line) and 11.2 BV/h (open circles, solid line). Continuous lines are model calculations.

Figure 10. Correlation of Na_2MoO_4 (circles)/NaOH (triangles) separation with the SRS model (dashed lines) and the rigorous model (solid lines). Adsorbent MN-270, T = 22 ^{o}C, $c_{Na2MoO4}^{0}$ = 0.50 mol/L, c_{NaOH}^{0} = 0.50 mol/L. Feed flow rate 5.0 BV/h, pulse volume 1.1 BV.

Scheme 1. Volumes and compositions of the streams in a simple two-column process. BV stands for the volume of the adsorbent bed.

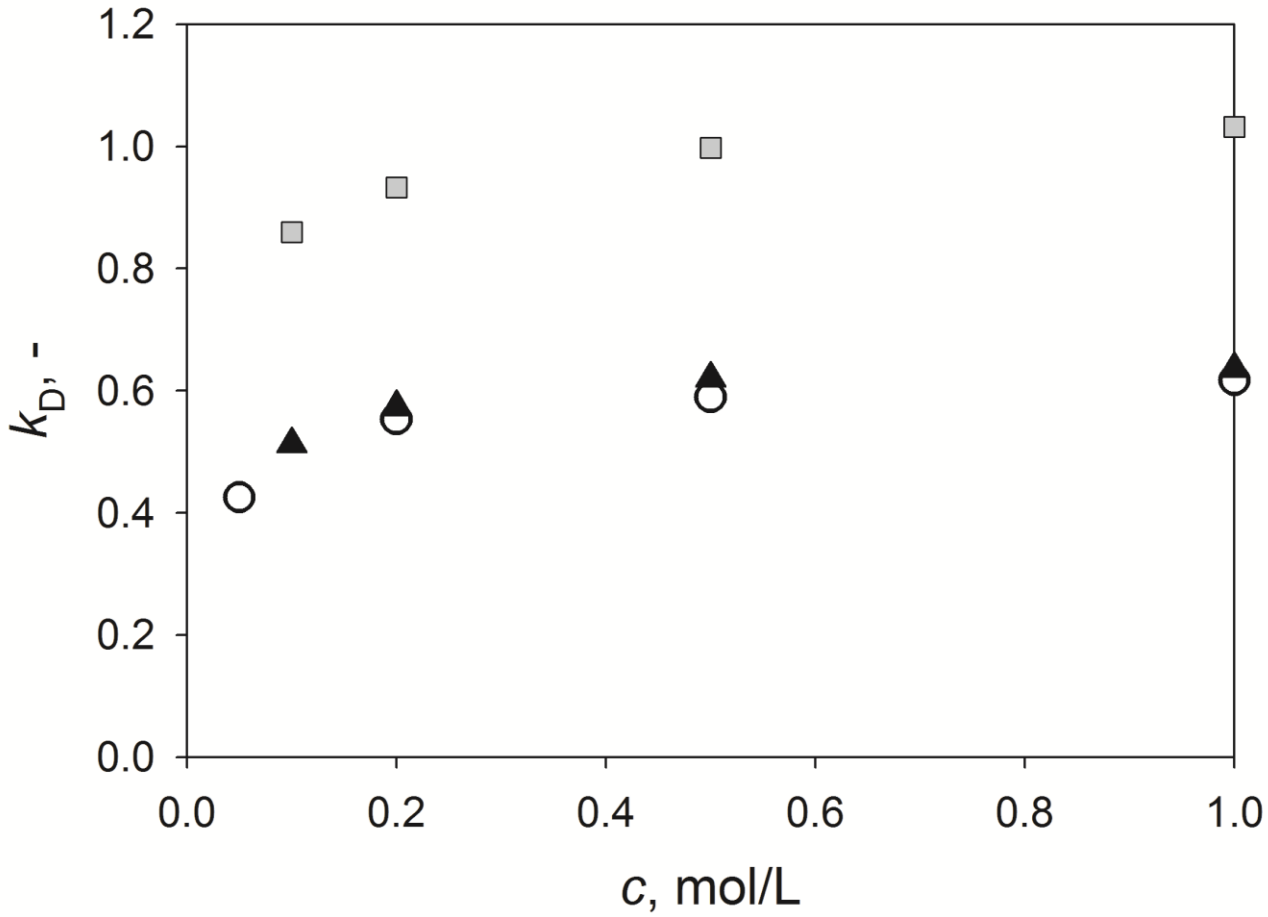

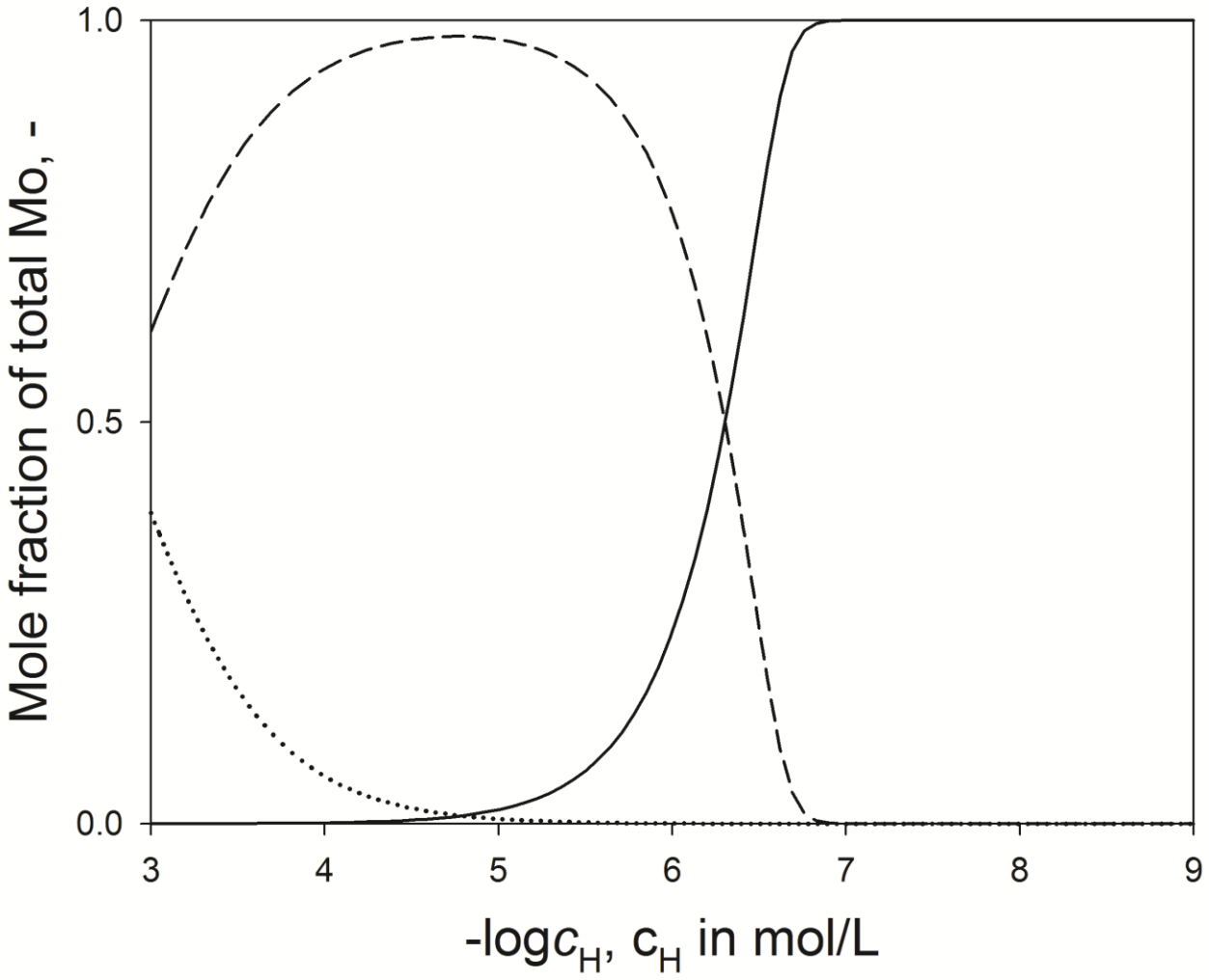

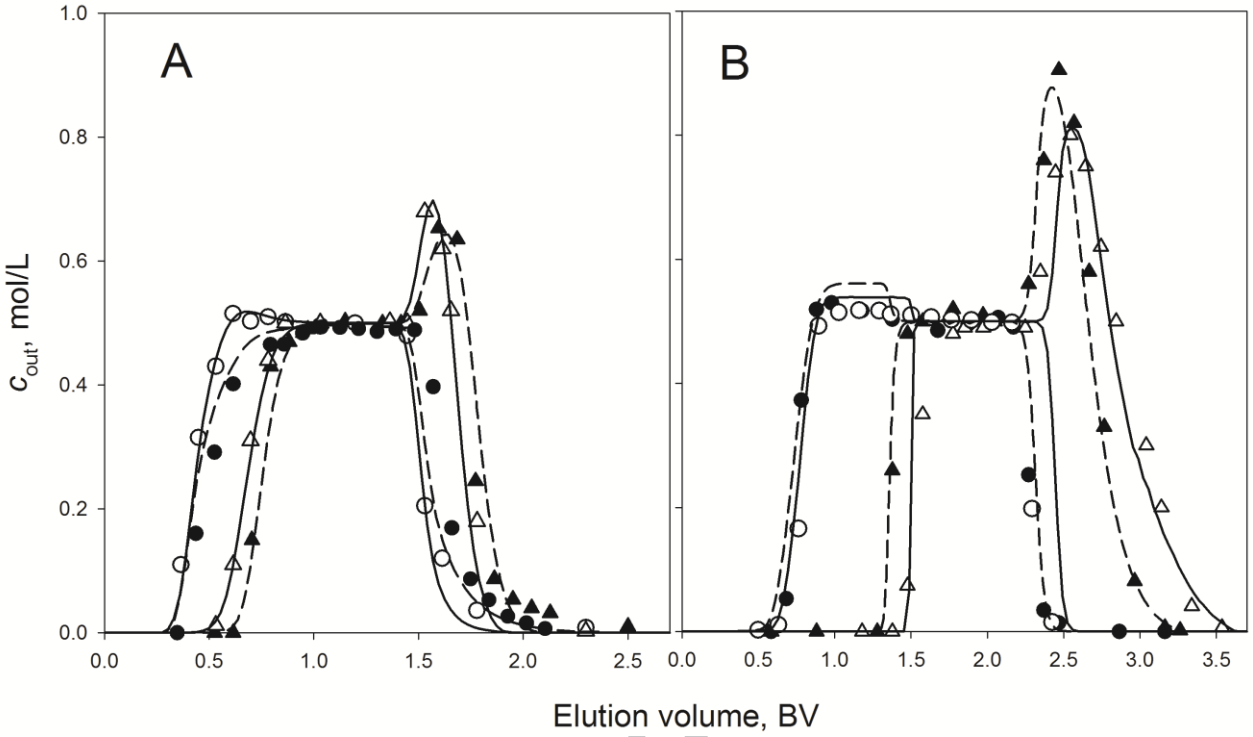

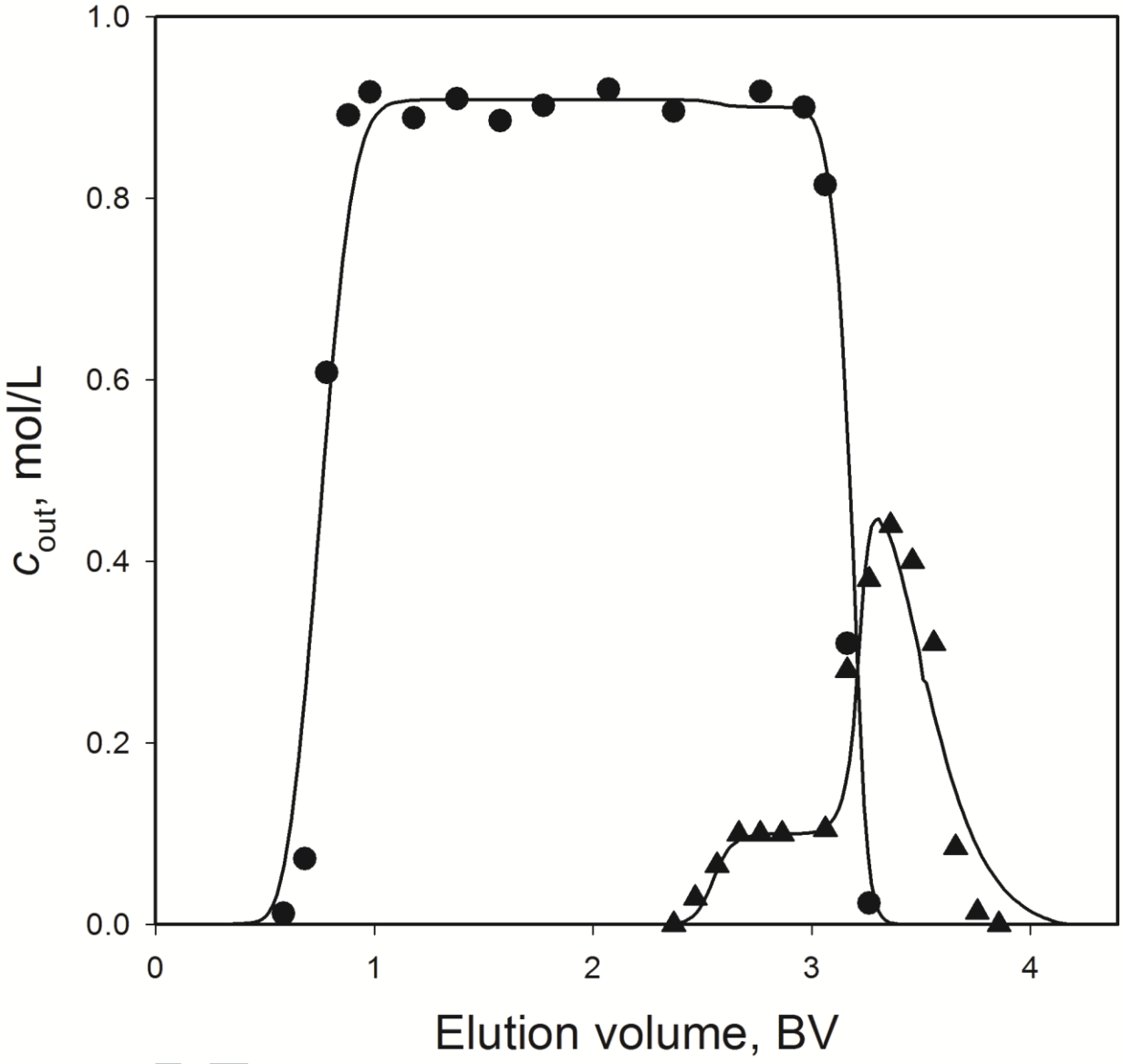
1.0
0.8
0.6
0.4
0.2
0.0
c_{out}, mol/L
0
1
2
3
4
Elution volume, BV

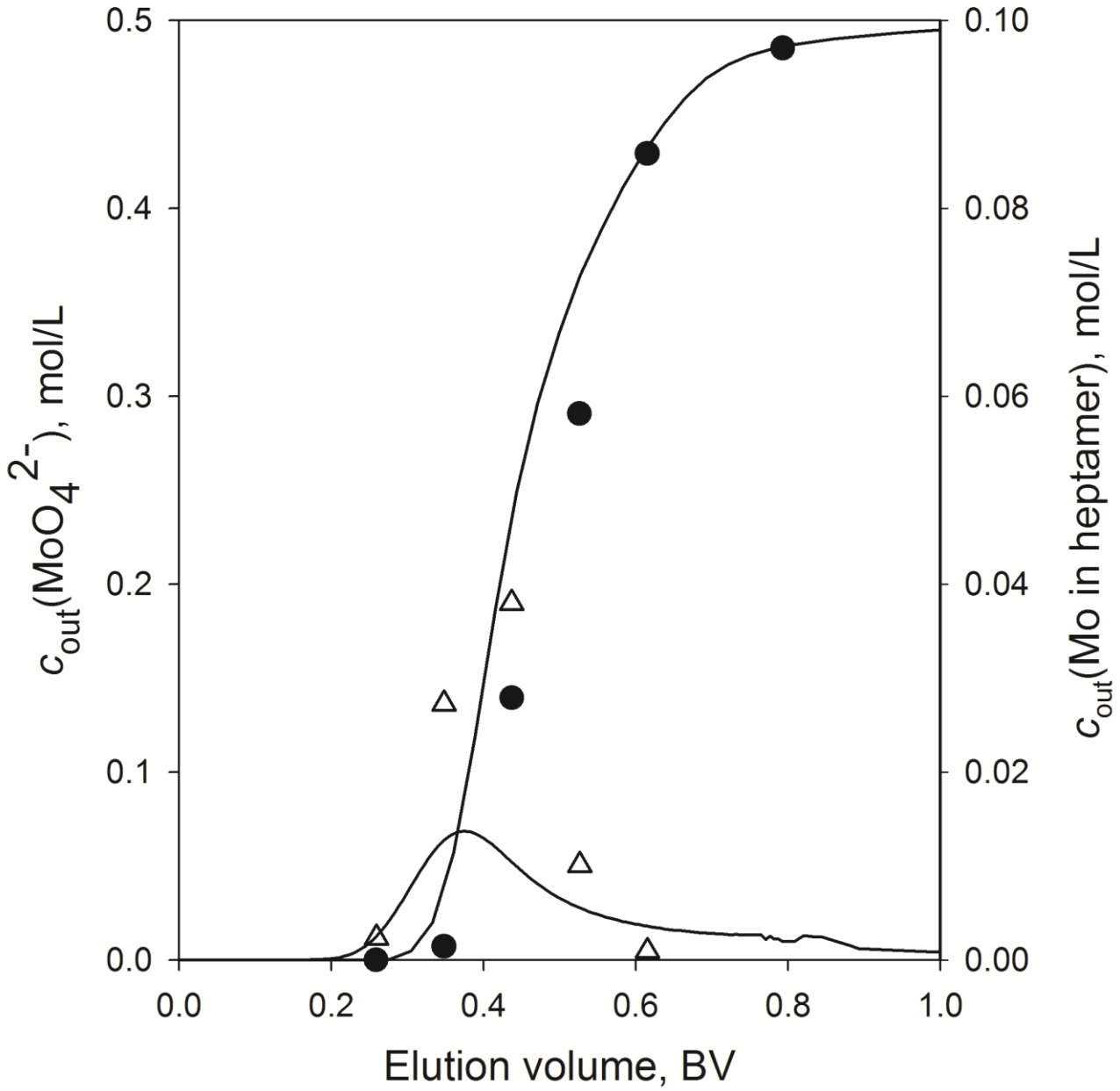
0.5
0.4
0.3
0.2
0.1
0.0
0.10
0.08
0.06
0.04
0.02
0.00
0.0
0.2
0.4
0.6
0.8
1.0
$c_{out}(MoO_4^{2-})$, mol/L
c_{out}(Mo in heptamer), mol/L
Elution volume, BV

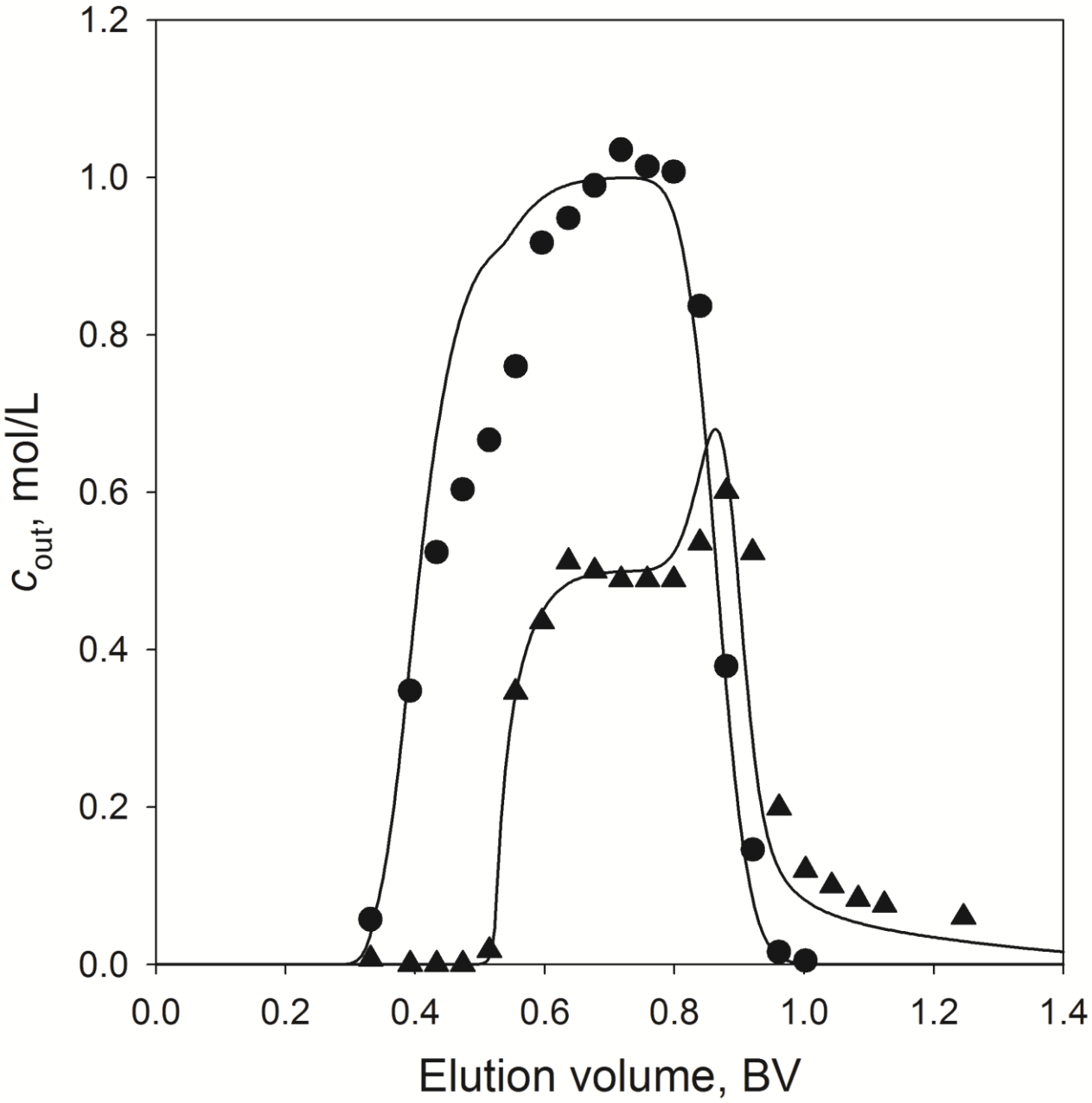

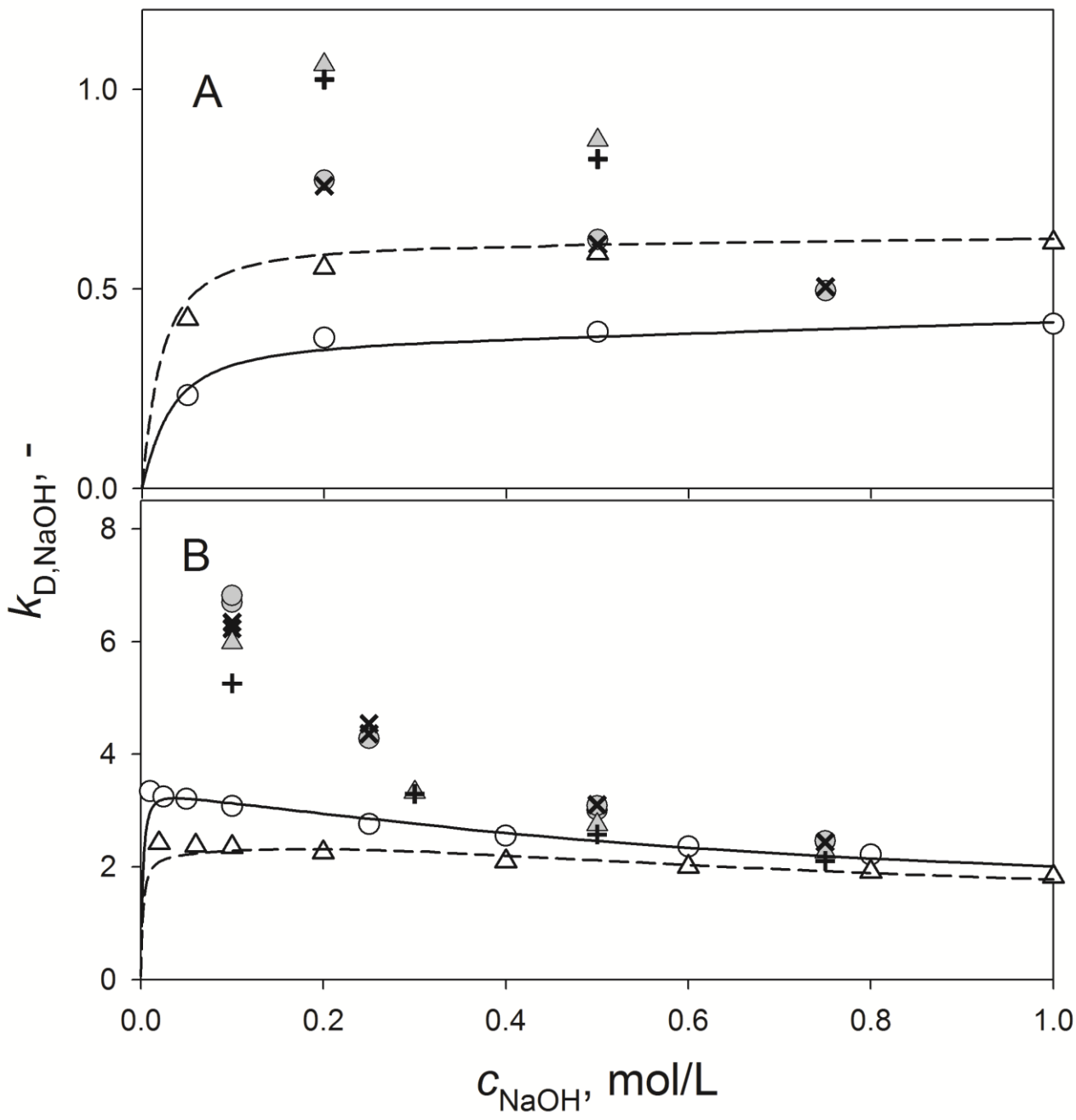
A
B
1.0
0.5
0.0
8
6
4
2
0
0.0
0.2
0.4
0.6
0.8
1.0
$k_{D,NaOH}$, -
c_{NaOH}, mol/L

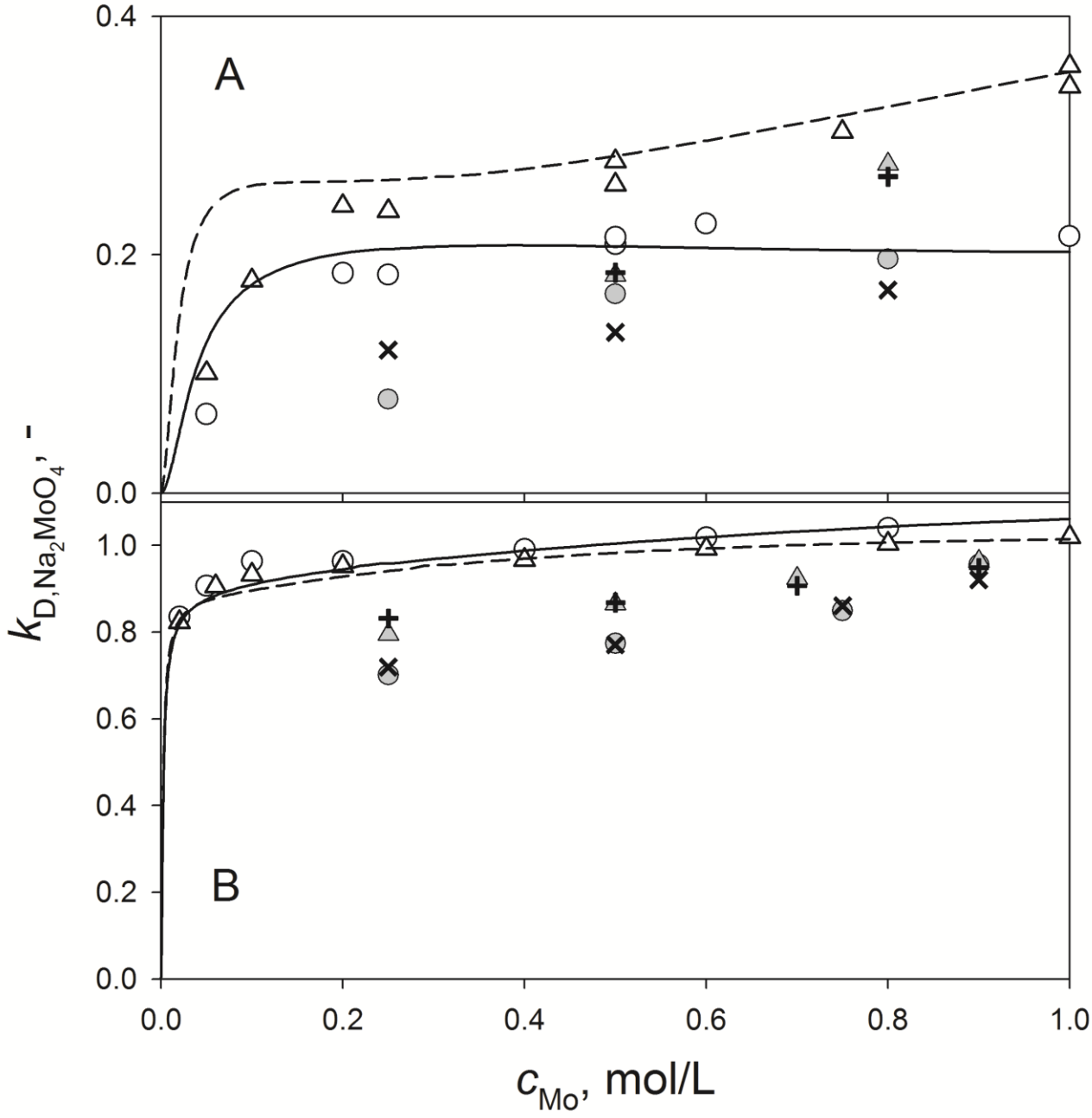
A
B
0.4
0.2
0.0
1.0
0.8
0.6
0.4
0.2
0.0
0.0
0.2
0.4
0.6
0.8
1.0
k_{D,Na_2MoO_4}, -
c_{Mo}, mol/L

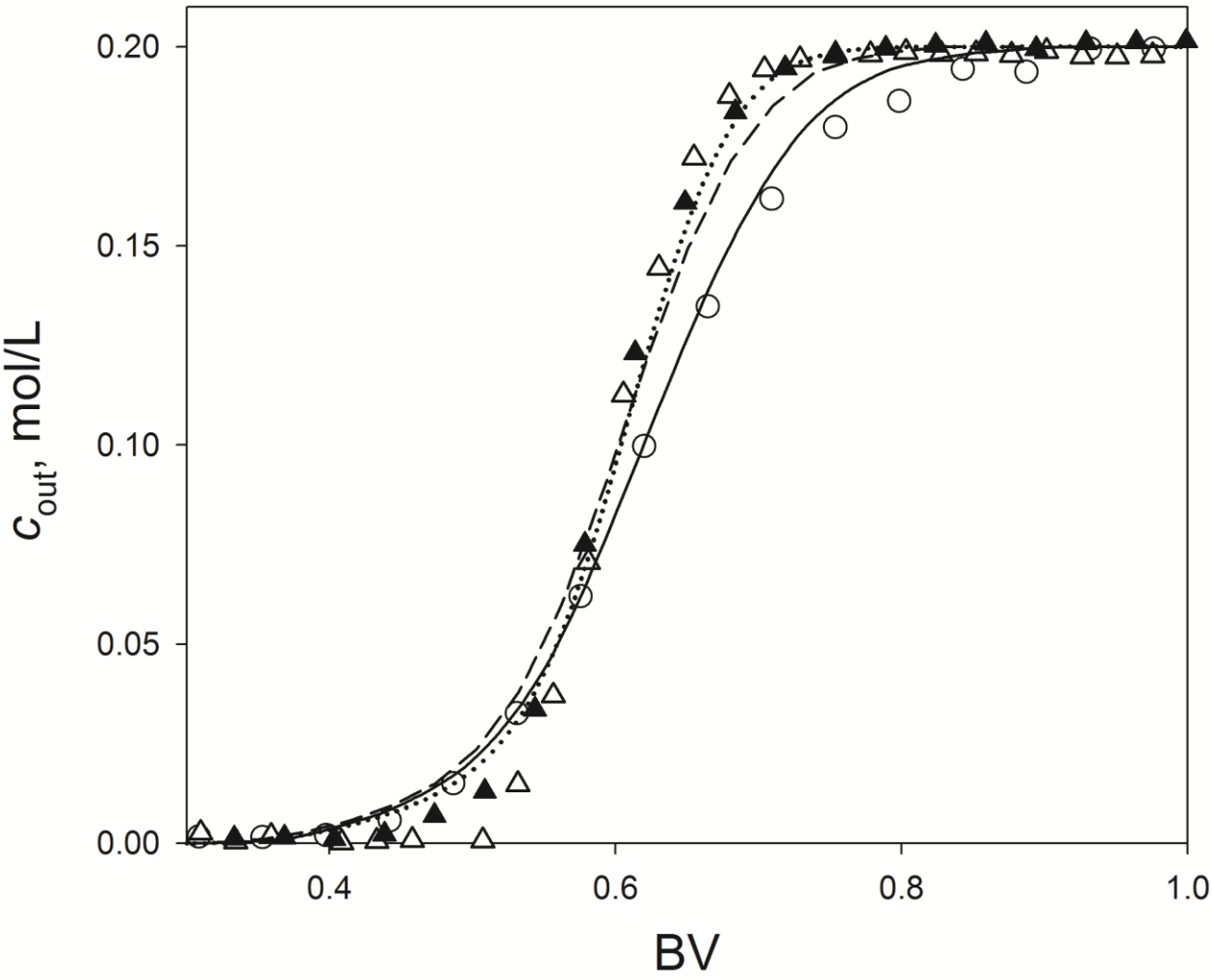

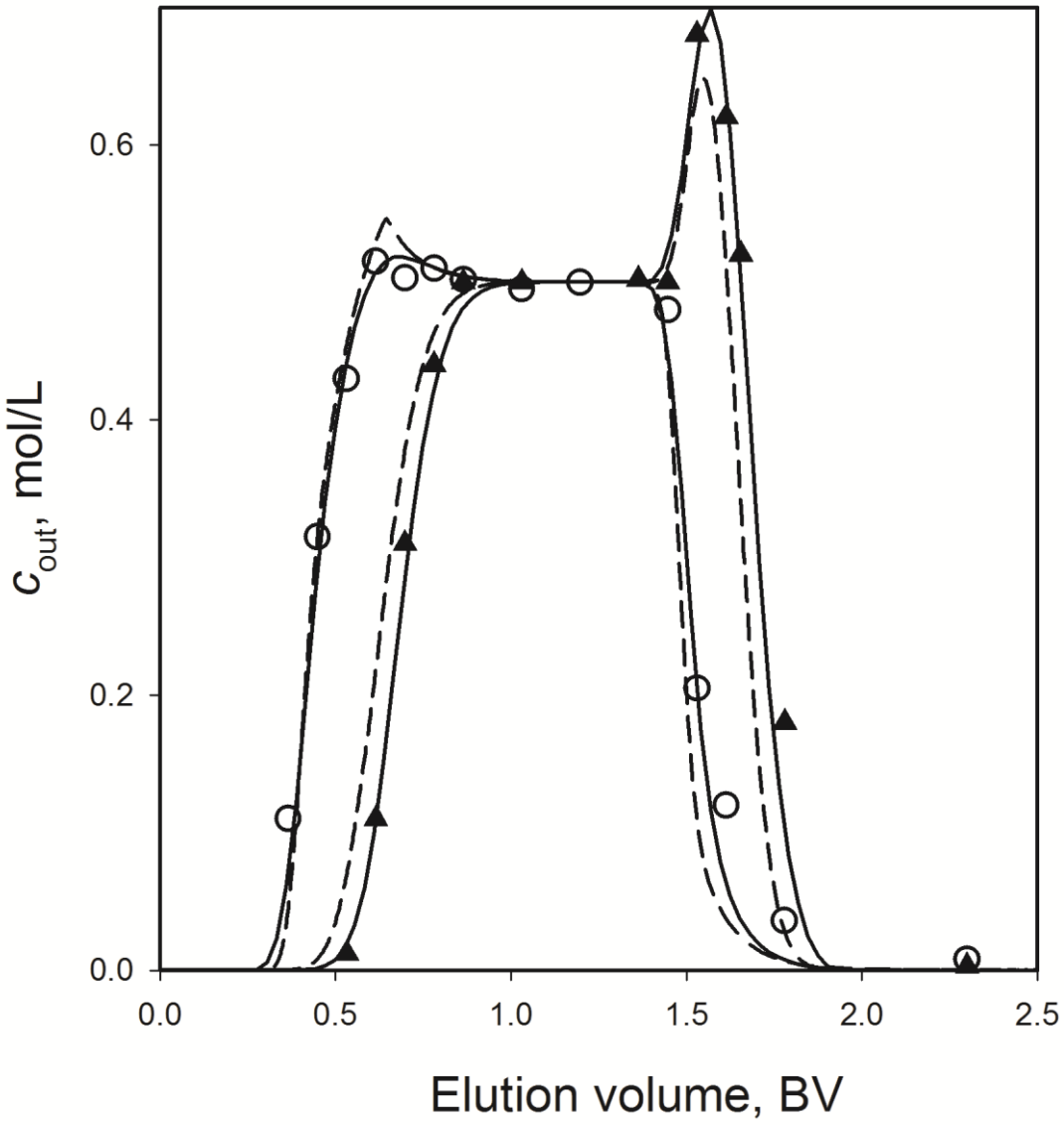

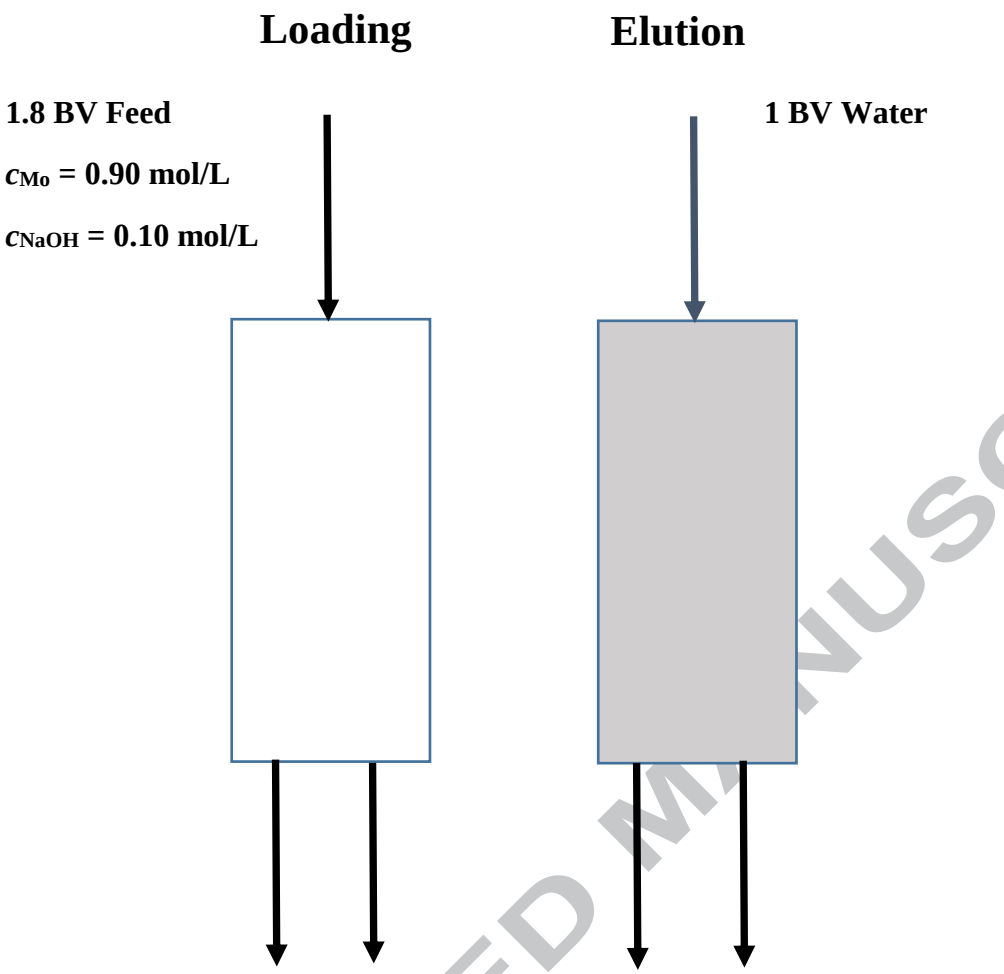

Highlights

- Non-ionic microporous adsorbents are used to separate Na_2MoO_4 and NaOH.
- Attractive rather than repulsive interactions gives better separation.
- Non-ionic cellulose adsorbent has better selectivity than charged adsorbents.
- Cooperative sorption model explains well the static and dynamic data.